THE JOURNAL OF PHYSICAL CHEMISTRY LETTERS
A JOURNAL OF THE AMERICAN CHEMICAL SOCIETY

pubs.acs.org/JPCL

Letter

First-Principles Demonstration of Nonadiabatic Thouless Pumping of Electrons in a Molecular System

Ruiyi Zhou, Dillon C. Yost, and Yosuke Kanai*

Cite This: *J. Phys. Chem. Lett.* 2021, 12, 4496–4503

Read Online

ACCESS | Metrics & More | Article Recommendations | Supporting Information

ABSTRACT: We demonstrate nonadiabatic Thouless pumping of electrons in *trans*-polyacetylene in the framework of Floquet engineering using first-principles theory. We identify the regimes in which the quantized pump is operative with respect to the driving electric field for a time-dependent Hamiltonian. By employing the time-dependent maximally localized Wannier functions in real-time time-dependent density functional theory simulation, we connect the winding number, a topological invariant, to a molecular-level understanding of the quantized pumping. While the pumping dynamics constitutes the opposing movement of the Wannier functions that represent both double and single bonds, the resulting current is unidirectional due to the greater number of double-bond electrons. Using a gauge-invariant formulation called dynamical transition orbitals, an alternative viewpoint on the nonequilibrium dynamics is obtained in terms of the particle-hole excitation. A *single* time-dependent transition orbital is found to be largely responsible for the observed quantized pumping. In this representation, the pumping dynamics manifests itself in the dynamics of this single orbital as it undergoes changes from its π bonding orbital character at equilibrium to acquiring resonance and antibonding character in the driving cycle. The work demonstrates the Floquet engineering of the nonadiabatic topological state in an extended molecular system, paving the way for experimental realization of the new quantum material phase.

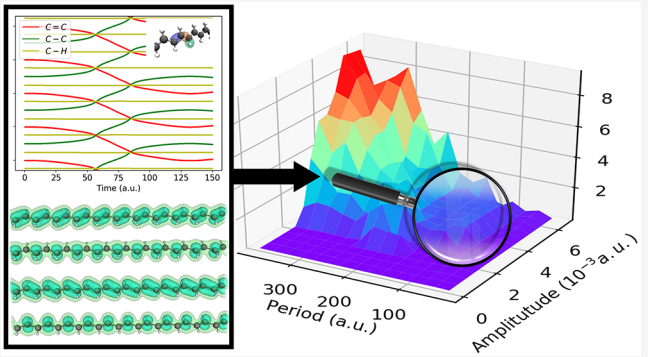

The quantized topological pumping phenomenon was first proposed by Thouless[1] in 1983 and is now widely referred to as Thouless pumping. Thouless's seminal work on the quantized particle transport in a slow varying potential showed that the quantization of the number of pumped particles derives from the topology of the underlying quantum-mechanical Hamiltonian, given by a Chern number. In recent years, Thouless pumping has been demonstrated experimentally in various systems[2,3] including an ultracold Fermi gas[4] and ultracold atoms in an optical lattice.[5] Most theoretical studies have employed model Hamiltonians[6−11] such as the Rice−Mele model,[12] and the description of topological pumping had assumed a complete adiabaticity of the Hamiltonian evolution. More recent work has begun to study the nonadiabatic effect in Thouless pumping.[13−15] In addition to studying the nonadiabatic effect on the otherwise adiabatic Thouless pump, nonadiabatic variance of Thouless pump has been proposed through setting up a periodically driven system. The idea of this so-called topological Floquet engineering is to use a time-periodic field to induce the topological properties in a driven system that is otherwise a trivial insulator.[16,17] In a Floquet system, the time-dependent Hamiltonian satisfies $\hat{H}(t + T) = \hat{H}(t)$ and the time-independent effective Hamiltonian can be defined from the evolution operator over one periodic T such that $\hat{H}_{eff}(\boldsymbol{k}) \equiv iT^{-1} \ln\left\{\hat{\mathcal{T}} \exp\left[-i\int_0^T dt\hat{H}(\boldsymbol{k}, t)\right]\right\}$. The term Floquet band engineering is often used to describe a theoretical approach that changes the topological properties of a system through the energy spectrum of the effective Hamiltonian. As discussed in the recent review by Rudner and Lindner,[17] for example, the topological Floquet band engineering aims to induce the nontrivial insulator phase by the use of a periodic driving field, whereas the system is in the trivial insulator phase without such a driving field. Nonequilibrium topological phenomena thus can be induced by applying time-periodic fields to the Hamiltonian. Nakagawa et al. studied different types of Floquet topological states for the periodically driven system in the nonadiabatic regime, and a nonadiabatic Thouless pump falls under the gapless Floquet topological state of Class A in one dimension.[18] The winding number is equal to the integrated particle current over the periodic time

Received: March 31, 2021
Accepted: May 3, 2021
Published: May 6, 2021

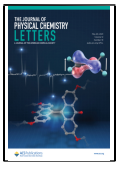

https://doi.org/10.1021/acs.jpclett.1c01037
J. Phys. Chem. Lett. 2021, 12, 4496–4503

T. The topological invariant is given in terms of the energy spectrum of the effective Floquet Hamiltonian, ε_i (quasienergy[19]), or equivalently in terms of the geometric phase

$$W = \int_{BZ} dk \sum_{i}^{Occ.} \frac{\partial \varepsilon_i(k)}{\partial k} = -\frac{1}{2\pi} \int_{BZ} dk \sum_{i}^{Occ.} \frac{\partial \gamma_i^{NA}}{\partial k} \tag{1}$$

where the nonadiabatic Aharonov−Anandan geometric phase[20] of the Floquet states $\Phi_i(k,t)$ is

$$\gamma_i^{NA}(k) \equiv \int_0^T dt \langle \Phi_i(k,t) | i\partial_t | \Phi_i(k,t) \rangle \tag{2}$$

Building on the work by Kitagawa et al.,[21] Nakagawa et al. showed that the winding number is also expressed as

$$W = \int_{BZ} dk \sum_{i}^{Occ.} \langle \Phi_i(k, t=0) | \hat{U}^{\dagger}(k) i\partial_k \hat{U}(k) | \Phi_i(k, t=0) \rangle \tag{3}$$

where $\hat{U}(k)$ is the Floquet operator (i.e., $\hat{U}(k) \equiv \hat{T} \exp[-i\int_0^T dt\, \hat{H}(k,t)]$).[18] This can be equivalently expressed in terms of the more familiar time-dependent Berry phase,

$$W = \frac{1}{2\pi} \sum_{i}^{Occ.} \left[\int_{BZ} dk \langle u_i(k, t=T) | i\partial_k | u_i(k, t=T) \rangle - \int_{BZ} dk \langle u_i(k, t=0) | i\partial_k | u_i(k, t=0) \rangle \right] \tag{4}$$

where $u_i(k,t)$ is the periodic part of the single-particle Bloch wave functions for an extended periodic system. Note that the Floquet state $\Phi_i(k,t)$ and $u_i(k,t)$ are related by $|u_i(k,t)\rangle = e^{-i\varepsilon_i(k)t} |\Phi_i(k,t)\rangle$. For Floquet topological states of a periodically driven system, the winding number is a nonzero integer, and the winding number can also be expressed, analogously to the static Chern insulator, as

$$W = C \equiv \frac{1}{2\pi} \int_0^T dt \int_{BZ} dk \sum_{i}^{Occ.} F_i(k,t) \tag{5}$$

where C is the first Chern number of the Floquet states and the generalized Berry curvature is given by $F_i(k,t) = i[\langle \partial_t u_i(k,t) | \partial_k u_i(k,t) \rangle - \langle \partial_k u_i(k,t) | \partial_t u_i(k,t) \rangle]$.[22] The Berry phase formulation is directly connected to the time-dependent Wannier functions, and the winding number can be interpreted as the number of the geometric centers of the Wannier functions (i.e., Wannier centers) pumped over one driving cycle in the Thouless pumping.[18,23] Note that the Wannier functions can be defined equivalently in terms of either $u_i(k,t)$ or Floquet states $\Phi_i(k,t)$ because they are related by a phase factor. Wannier centers have already been used in the literature for characterizing topological insulators in the adiabatic description.[8,23] In the recent work by Yost et al.,[24] we introduced the nonadiabatic dynamics of maximally localized Wannier functions[25,26] in real-time time-dependent density functional theory (RT-TDDFT), and its application to studying Thouless topological charge pumping was briefly discussed. The winding number can be conveniently expressed in terms of the time-dependent maximally localized Wannier functions (MLWFs), $w_i(r,t)$, as

$$W = L^{-1} \sum_{i}^{Occ.} [\langle w_i(t=T) | \hat{r} | w_i(t=T) \rangle - \langle w_i(t=0) | \hat{r} | w_i(t=0) \rangle] \tag{6}$$

due to the Blount identity $\langle w_i(t) | \hat{r} | w_i(t) \rangle = \frac{L}{2\pi} \int_{BZ} dk \langle u_i(k,t) | i\partial_k | u_i(k,t) \rangle$, the position operator here is defined according to the formula given by Resta for the extended periodic systems.[27] In this work, we study whether nonadiabatic Thouless pumping, a Floquet topological state, can be observed for electrons in a real molecular system. We demonstrate the nonadiabatic Thouless pumping of electrons in a *trans*-polyacetylene polymer, using time-dependent first-principles electronic structure theory. *Trans*-polyacetylene represents a chemical exemplification of the classic Su-Schrieffer-Heeger (SSH) model which is widely used to study the transition between topological insulator and normal/trivial insulator phases by artificially changing the empirical hopping parameters between the single and double C−C bonds in this Peierls distorted system.[28] The two distinct carbon atom sites from the Peierls instability give rise to the chiral (i.e., sublattice) symmetry in the Hamiltonian.

We apply a time-dependent electric field as the driving field with a specific period (i.e., frequency) along the polymer direction. The electron current is directly obtained from the flux of the geometric centers of the time-dependent MLWFs. Computational details are given in the Computational Methods section. In the context of Floquet theory, the initial state must return to the same Hilbert subspace of the Floquet operator after a driving period. This is not the adiabatic evolution condition, and particle-hole excitations are still allowed in this formulation as discussed by Nakagawa et al.[18] This aspect is also relevant for discussing the applicability of the Floquet theory to time-dependent density functional theory (TDDFT).[29−32] The Kohn−Sham Hamiltonian depends on the time-dependent electron density even when the adiabatic approximation is adapted for the exchange-correlation potential and the dependence on the initial state is consequently neglected.[33,34] Therefore, the Hamiltonian is time-periodic (i.e., Floquet theory is applicable) only if the original electron density is recovered after each driving cycle is completed. We can quantify the extent to which the Floquet theorem is satisfied by calculating the determinant of the overlap matrix, S, between the initial time-dependent Kohn−Sham (TD-KS) orbitals and those after one driving cycle has passed as shown in Figure 1. Dark shaded areas with values close to one satisfy this condition and the Floquet theory is applicable, and the integrated current over one driving cycle is equal to the winding number.

In the low frequency regime (e.g., T = 1000 au) toward the adiabatic evolution limit (Figure 2), particle-hole excitations are not possible, given the much larger energy gap of 2.02 eV, which corresponds to the electric field with T = 84.6 au. Below a certain electric field amplitude ($\sim 4 \times 10^{-3}$ au), the overlap matrix determinant is essentially one, indicating the original electron density is recovered after one driving cycle as seen in Figure 2. However, this is solely because the electron current is absent. At the same time, when the field amplitude exceeds the threshold, Zener tunneling is possible in the extended systems; it causes the electrical breakdown, resulting in a very large current (Figure 2). The electron density, however, does not return to its initial state after one driving cycle, and the overlap

https://doi.org/10.1021/acs.jpclett.1c01037
J. Phys. Chem. Lett. 2021, 12, 4496−4503

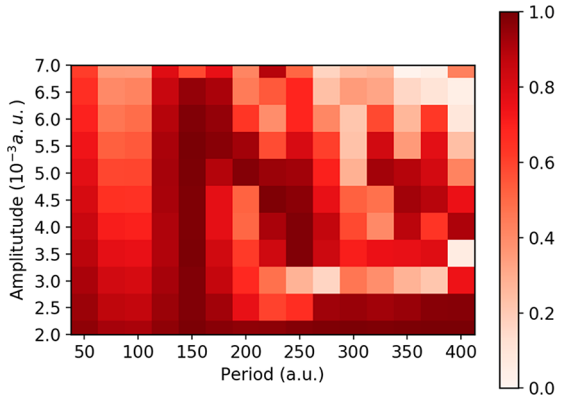

Figure 1. Determinant of the overlap matrix, S, between the initial and final TD-KS states in a single driving cycle as a function of the driving field period and amplitude, sampled at uniform intervals of 25 au and 0.5×10^{-3} au, respectively.

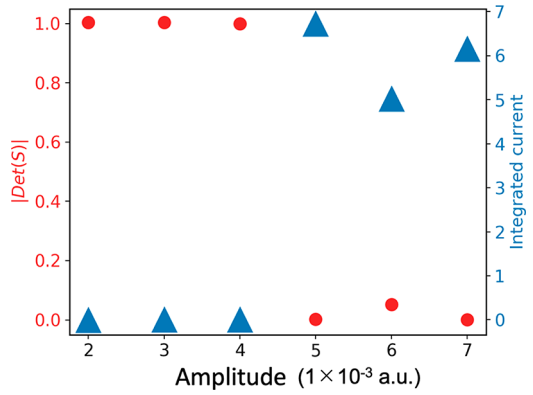

Figure 2. Determinant of the overlap matrix between the initial and final TD-KS states after a single driving cycle (left) and the integrated current per one C−C monomer unit (right) for the driving field period of T = 1000 au as a function of the driving field amplitude.

matrix determinant is therefore not close to one (see Figure 1). The Zener tunneling is observed above the threshold field amplitude but not the topological pump.

For various combinations of the period (50−400 au) and amplitude ($2-7 \times 10^{-3}$ au) of the driving field, Figure 3 (left) shows the integrated electron current per C−C monomer unit over one driving cycle. In order for the integrated current over one driving cycle to be identified as the winding number, the Floquet condition must be satisfied such that the overlap matrix determinant is unity. Figures 1 and 3 show that the Floquet topological state is obtained for some combinations of the driving field period and amplitude. First, the overlap matrix determinant must be one so that the time-dependent electron density returns to its original state after one driving period. This is a necessary condition for the winding number formulation as the Floquet theorem is applied to TDDFT because the Hamiltonian depends on the electron density. At the same time, the winding number itself must be a nonzero value for the Floquet topological state. As indicated by the enclosed squares in Figure 3 (right), certain combinations of the period and amplitude yield the required features of the Floquet topological state. Since the overlap matrix determinant is never exactly one in numerical simulations, we indicate the areas that show the overlap matrix determinant value of ≥0.96 with a non-negligible electron current. For the Floquet topological state indicated by these enclosed squares, the integrated current per driving cycle is given by the winding number and an integer value is expected. While the numerical simulation does not give exactly an integer number here, the computed values show a discrete quantization expected for the integrated current, effectively yielding the winding number of one, two, or three in the areas where the Floquet condition is satisfied.

Having a Floquet topological state identified for this real molecular system with certain driving periods and amplitudes, we now study the nature of the electron current in the Floquet topological state. While the winding number is the physical observable here, orbital analysis of the simulation enables us to gain chemical insights into the dynamics of the nonadiabatic topological pump.[35] As discussed by Nakagawa et al.,[18] the

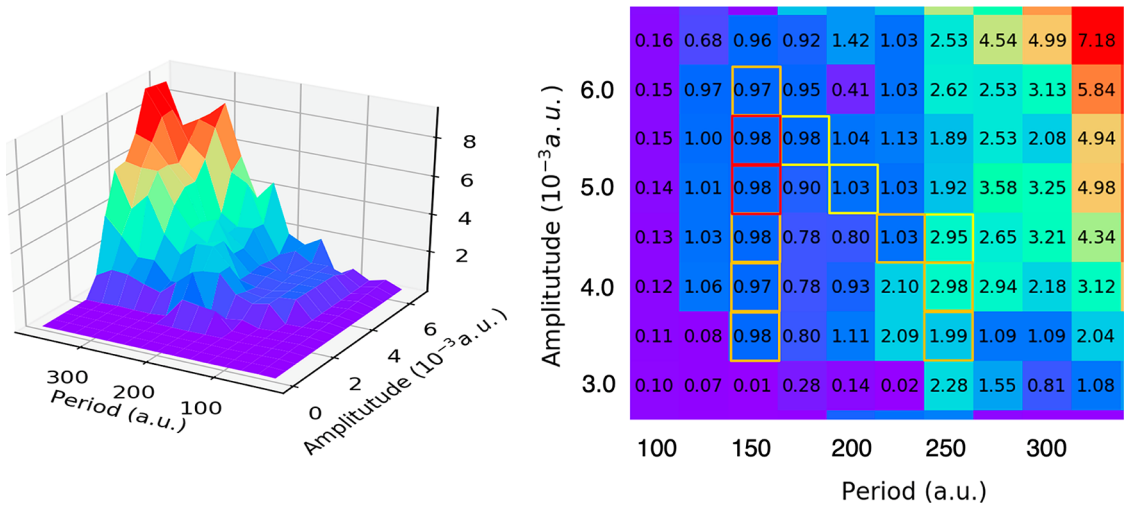

Figure 3. (Left) Integrated current over one driving cycle per C−C monomer unit, as a function of the driving field period and amplitude, sampled at uniform intervals of 25 au and 0.5×10^{-3} au, respectively. (Right) The integrated current values are shown, and the areas with the overlap matrix determinant close to one are indicated by three colored squared boxes: Det(S) ≥ 0.99 (red), ≥0.98 (orange), and ≥0.96 (yellow). See also Figure 1. We also provide the figure in the units of femtosecond (period) and of V/m (amplitude) in the Supporting Information.

https://doi.org/10.1021/acs.jpclett.1c01037
J. Phys. Chem. Lett. 2021, 12, 4496−4503

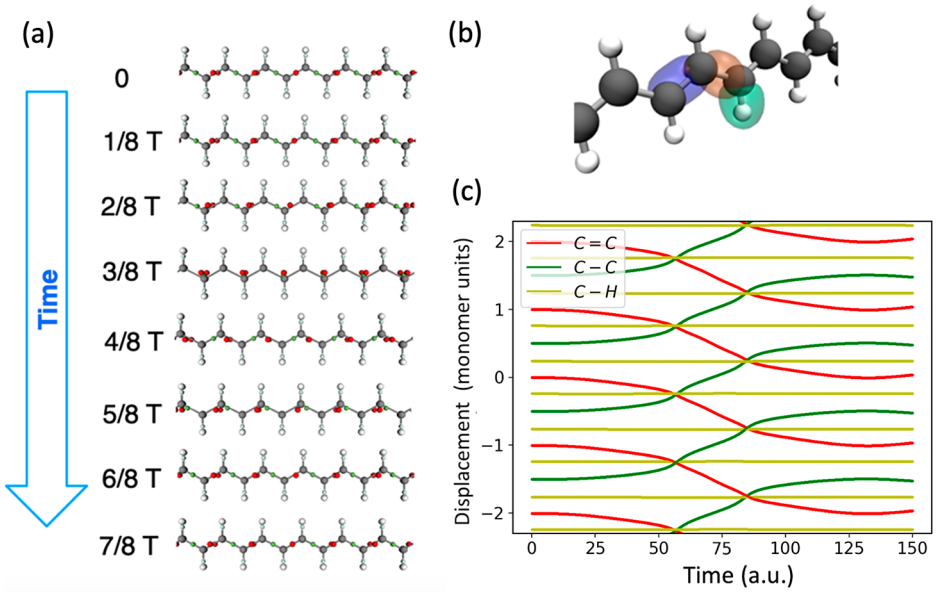

Figure 4. Wannier dynamics observed for the winding number of one ($W = 1$) with the driving field period of 150 au and the field amplitude of 4×10^{-3} au. (a) Snapshots of the geometric centers of the MLWFs (Wannier centers) at different instances of time in a single driving cycle. (b) Electron density isosurface of the MLWFs that correspond to the double and single C−C bonds as well as for the C−H bonds. (c) The movement of the Wannier centers are shown as points.

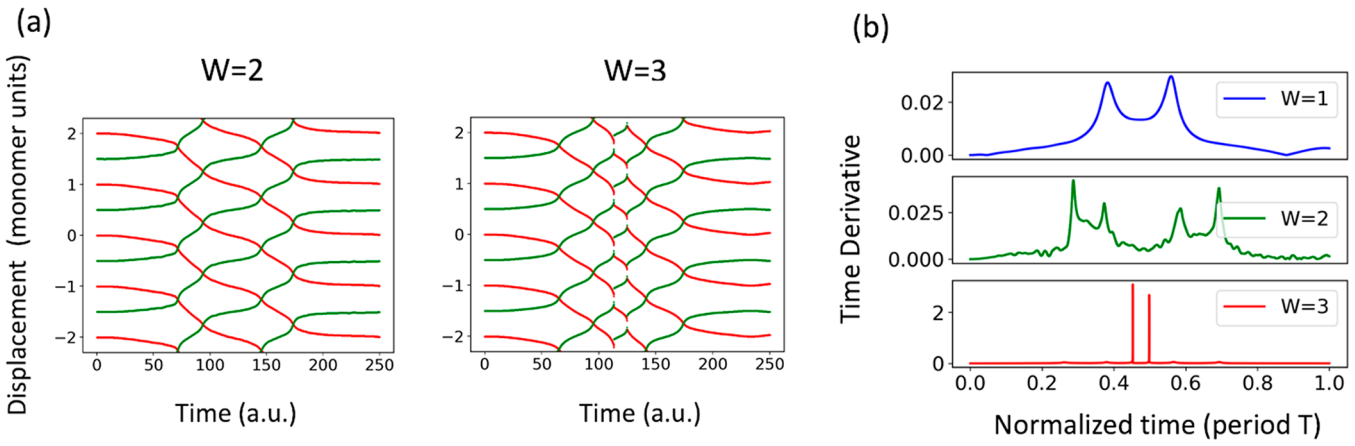

Figure 5. Wannier dynamics observed for the winding numbers two ($W = 2$) and three ($W = 3$) with the driving field period of 250 au and the field amplitudes of 3.5×10^{-3} au for $W = 2$ (left) and 4×10^{-3} au for $W = 3$ (right). (a) Movement of the Wannier centers shown as points for the double (shown in red) and single (shown in green) C−C bonds. (b) Time derivative of the Wannier center displacements for $W = 1$, 2, and 3.

winding number can be interpreted as the number of the Wannier centers pumped over one driving cycle in the Thouless pumping. As can be seen in Figure 4, individual monomer units show two and one MLWF for the double and single C−C bonds, respectively. Each MLWF represents two electrons of the opposite spins. In the equilibrium ground state, the Wannier function spreads for the double and single C−C bonds are 2.32 and 1.78 au^2, respectively. The time-dependent MLWFs remain highly localized; the mean double-bond Wannier spreads are 2.3−3.4 au^2, and the single-bond Wannier spreads are 1.7−1.9 au^2, depending on the field amplitude and period (see the Supporting Information). Let us now discuss the pumping behavior for the winding number of one, $W = 1$. As a representative case, we analyze the particular condition with the field period = 150 au and amplitude = 4×10^{-3} au, which gives the integrated current of 0.97e numerically (per driving cycle per C−C monomer unit). The time-dependent MWLFs remain highly localized during the nonequilibrium dynamics; the average spread values of the double- and single-bond MLWFs do not increase above 3.0 and 1.9 au^2, respectively. Figure 4 shows time-dependent changes of the Wannier centers over one period. The MLWFs that correspond to C−H bonds remain essentially unchanged. All the Wannier centers remain oscillating back and forth when the electron current is absent (see the Supporting Information). While both of the two double-bond Wannier centers move in one direction, the single-bond Wannier centers move in the opposite direction, resulting in the overall directional transport with the winding number of one. At the same time, the MLWF dynamics do not yield a conceptually simple description of C−C bond electrons being pumped in one direction as in the SSH model. There are instances at which all MLWFs localize in the vicinity of a carbon atom as seen at $t = 3/8T$ in Figure 4a.

The driving field period = 250 au with the amplitude = 3.5×10^{-3} au yields the winding number of two ($W = 2$, 1.99

https://doi.org/10.1021/acs.jpclett.1c01037
J. Phys. Chem. Lett. 2021, 12, 4496−4503

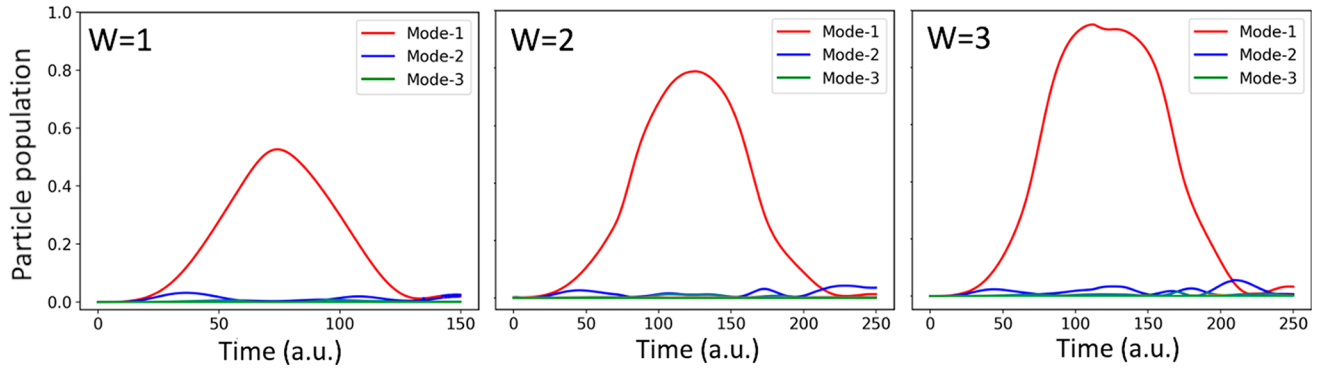

Figure 6. Time-dependent particle population, $b_i(t)^2$ in eqs 7 and 8, in the natural transition orbitals with the three most significant contributions for $W = 1$ (period = 150 au, amplitude = 4×10^{-3} au), $W = 2$ (period = 250 au, amplitude = 3.5×10^{-3} au), and $W = 3$ (period = 250 au, amplitude = 4×10^{-3} au) cases.

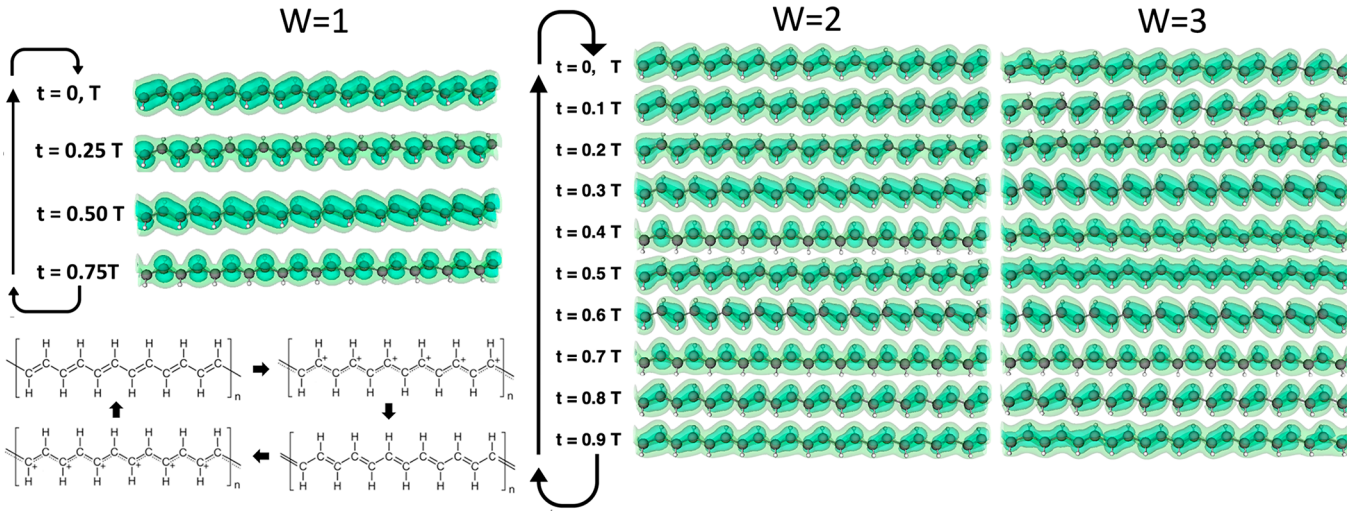

Figure 7. Isosurface of the time-dependent natural transition orbital with the most significant change (see Figure 6) for the $W = 1$ (period = 150 au, amplitude = 4×10^{-3} au), $W = 2$ (period = 250 au, amplitude = 3.5×10^{-3} au), and $W = 3$ (period = 250 au, amplitude = 4×10^{-3} au) cases. The videos of this dynamical change are provided in the Supporting Information for convenience.

numerically), and the winding number of three ($W = 3$, 2.98 numerically) is obtained with the driving field period = 250 au and amplitude = 4×10^{-3} au. The corresponding Wannier center movement shows that they are pumped over a multiple number of C−C monomer units, given by the winding number (see Figure 5a). The MLWF dynamics still uphold the molecular description such that only single and double bonds are formed alternatively on the C−C units while the winding number itself does not mathematically impose such a physical condition (see the Supporting Information). As can be seen in Figure 5a, the Wannier center movement shows a behavior that is much more complex than the case for $W = 1$ (Figure 4). The movement of the Wannier centers increases rapidly in the middle of the driving cycle. Particularly for the $W = 3$ case, the Wannier centers exhibit a small but abrupt jump around the middle of the driving cycle as evidenced in the time derivative of the Wannier center positions (see Figure 5b). At the same time, the spreads of the MLWFs remain rather well localized (see the Supporting Information). A similar behavior was seen in our earlier work[24] in which a discontinuous movement of the Wannier centers was also observed but in a different context (i.e., optically gated transistor setup with time-independent homogeneous electric field and optical-excitation field). To summarize our observation here, the winding numbers larger than one, $W > 1$, do not imply a simple repetition of the $W = 1$ pumping over the C−C monomer units by an integer number of times, given by the winding number (e.g., two and three here). This point is further evidenced in the following by studying the pumping dynamics in terms of the particle-hole excitation.

While the winding number formulation through the Wannier function is intuitive due to having the localized description of electrons, an alternative viewpoint of this nonadiabatic Thouless pump can be developed by studying the nonequilibrium dynamics in terms of the particle-hole excitation dynamics. In the recently introduced dynamical transition orbital (DTO) approach, the RT-TDDFT simulation is framed in a new set of the gauge-invariant time-dependent orbitals.[36] Within this DTO gauge, the particle-hole excitation dynamics is obtained by formulating the individual orbitals as a linear combination of the hole and particle orbitals,

$$|\psi_i^{DTO}(t)\rangle = a_i(t)|\psi_i^h(t)\rangle + b_i(t)|\psi_i^p(t)\rangle_{i=1\ldots N_{Occ.}} \quad (7)$$

where $|\psi_i^h(t)\rangle$ and $|\psi_i^p(t)\rangle$ are the hole and particle orbitals, respectively. The real-valued expansion coefficients satisfy

$$a_i(t) \geq 0, \quad b_i(t) \geq 0, \quad a_i(t)^2 + b_i(t)^2 = 1 \quad (8)$$

https://doi.org/10.1021/acs.jpclett.1c01037
J. Phys. Chem. Lett. 2021, 12, 4496−4503

The particle and hole orbitals are essentially time-invariant here (up to the phase) while the hole and particle coefficients vary in time. Figure 6 shows the particle population, $b_i(t)^2$, in eqs 7 and 8 for three DTOs with the most dominant changes. Interestingly, a *single* DTO is predominantly responsible for the nonequilibrium dynamics for all the cases. By projecting this particular DTO onto reference Kohn−Sham eigenstates, one finds that the constituting hole and particle orbitals largely derive from degenerate HOMOs and degenerate LUMOs, respectively. Therefore, these particular orbital dynamics, into which the pumping dynamics manifests itself, represents π bonds at equilibrium initially at $t = 0$. In contrast to the dynamics of MLWFs, a conceptually simple understanding of the Thouless pump can be obtained by studying solely the dynamical change of this particular transition orbital. For the $W = 1$ case as a representative example, Figure 7 shows that this orbital evolves from being localized on the typical C−C double bonds as the π bonding state into a resonance state before localizing again but on the other alternating set of C−C bonds at $t = 0.5T$, exhibiting a significant π *antibonding* character. Then, it continues to evolve into another resonance state before it returns again as the π -bonding orbital on the C−C double bonds. Pendás et al. have previously discussed how topological invariant properties can be rationalized in terms of such a chemically intuitive description,[37] and a simple schematics can depict the $W = 1$ dynamics as shown in Figure 7. Similar DTO dynamics can be observed for the $W = 2$ and 3 cases but with more rapid changes in the midst of the driving cycle. This is in accordance with the Wannier dynamics that show more rapid changes in the middle of the driving cycle (Figure 5). As seen in the Wannier center dynamics (Figure 5), the $W = 2$ and 3 cases do not represent a simple repetition of the $W = 1$ transition orbital changes. Indeed, all three cases show varying dynamics for the transition orbital in terms of the particle occupation change in a single driving cycle (Figure 6). For $W = 2$, similarly to the $W = 1$ case, the transition orbital gains resonance character before $t = 0.3T$, antibonding character at $t = 0.3$T, and then another resonance character at $t = 0.4T$ (Figure 7). The transition orbital then repeats the visually similar changes in the second half of the driving cycle. The $W = 3$ case is qualitatively dissimilar to the $W = 1$ or $W = 2$ cases. The transition orbital gains the resonance character at $t = 0.2T$ and antibonding character at $t = 0.3T$. However, change to another resonance state character is not observed until much later, $t = 0.7T$. The transition orbital undergoes visibly small changes for $t = 0.3-0.7T$ in the driving cycle, and the fact that the winding number is three is not obvious or intuitive from the dynamical changes of this transition orbital. Although the winding number can be interpreted as the number of the Wannier centers pumped over one driving cycle,[18] the changes in the dynamical transition orbital cannot be interpreted straightforwardly in relation to the winding number. At the same time, in this dynamical transition orbital gauge, a single orbital effectively captures the pump dynamics, and its changes are more intuitive from the viewpoint of understanding the dynamics in terms of an electron transition among the familiar chemical bonding orbitals.

Using first-principles, time-dependent, electronic structure theory, we demonstrated nonadiabatic Thouless pumping of electrons in *trans*-polyacetylene in the framework of Floquet engineering. Using an external electric field as the driving field for the time-dependent Hamiltonian, we identified the regimes in which the quantized pump is operative as a function of the driving field period (frequency) and amplitude. By employing the time-dependent maximally localized Wannier functions in real-time time-dependent density functional theory simulations, we connect the winding number formulation by Nakagawa et al.[18] to a molecular-level understanding of this Thouless pump. These pumping dynamics are described by the movement of the Wannier functions that represent both C−C double bonds and single bonds but not C−H bonds. While the Wannier centers move in opposite directions, having more electrons in the double bonds than in the single bonds results in a net unidirectional current overall. The direction of the current is governed by the initial polarization direction of the applied time-dependent electric field. Although the topological invariant, the winding number, specifies the number of C−C monomer units the electrons are pumped over in a single driving cycle, the Wannier dynamics shows that the rate at which the electrons are pumped is not uniform during the driving cycle for the cases with larger winding numbers of two and three. Using a gauge-invariant formulation of the occupied time-dependent Kohn−Sham orbitals called dynamical transition orbitals,[36] a *single* time-dependent orbital is found to be responsible for the observed Thouless pumping. The pumping dynamics manifest in the dynamic changes of this single transition orbital that characterizes the π bonding at equilibrium, and it undergoes changes to acquire resonance and antibonding character in the driving cycle. Having the dynamics formulated in terms of the particle-hole transition, it was further shown that the larger winding numbers of two and three do not indicate a simple repetition of the $W = 1$ pumping over C−C monomer units by two and three times as the electrons are pumped over two and three C−C monomer units, respectively. Topological insulators are generally studied in terms of electronic structure in a static field of the fixed-position nuclei; how lattice dynamics of nuclei influence the exotic transport behavior at room temperature is of great importance for experimental realization and for practical application of quantum materials. This aspect is particularly relevant for the present case because the topological properties are not guaranteed to be robust in the nonadiabatic regime, including Floquet topological states.[17] Investigation into the lattice dynamics and thermal effects will be pursued in a future work.

COMPUTATIONAL METHODS

Real-time time-dependent functional theory (RT-TDDFT)[29,38] has become an increasingly popular method for studying out-of-equilibrium electronic structures in the past few decades,[39,40] including those of topological materials.[24,41,42] RT-TDDFT simulation was performed using the Qb@ll branch[43] of Qbox code[44] within a plane-wave pseudopotentials (PW−PP) formalism.[45] We employed a 55-atom supercell (11 C−C monomer unit cells aligned along the x axis) with the periodic boundary condition (51.32 Bohr ×15.0 Bohr ×15.0 Bohr) and the Γ-point approximation in the Brillouin zone integration. The molecular geometry (bond lengths, bond angles, and the lattice constant) of the *trans*-polyacetylene was taken from that of experiments[46] and is included in the Supporting Information. All atoms were represented by Hamann−Schluter−Chiang−Vanderbilt (HSCV) norm-conserving pseudopotentials,[47,48] and the PBE[49] generalized gradient approximation exchange-correlation functional was employed with the plane-wave cutoff energy of 40 Ry for the Kohn−Sham orbitals. For the time-

https://doi.org/10.1021/acs.jpclett.1c01037
J. Phys. Chem. Lett. 2021, 12, 4496−4503

dependent Kohn−Sham equation, the maximum localized Wannier functions (TD-MLWF) gauge was used and a time-dependent electric field was applied using the length gauge as discussed in ref 24. The enforced time-reversal symmetry (ETRS) integrator[50] was used with the integration step size of 0.1 au. The simulations were performed with the applied electric as the driving field with a field period range of 50−400 au and amplitude range of $2-7 \times 10^{-3}$ au at uniform intervals of 25 au and 0.5×10^{-3} au, respectively.

■ ASSOCIATED CONTENT

Supporting Information

The Supporting Information is available free of charge at https://pubs.acs.org/doi/10.1021/acs.jpclett.1c01037.

Determinant of overlap matrix, integrated current, averaged MLWF spreads, time-dependent change of the MLWF spreads, movement of Wannier function centers, resonance structure schematics of the dynamical transition orbital, and molecular geometry (PDF)

Video of the dominant dynamical transition orbital changes for $W = 1$ (MPG)

Video of the dominant dynamical transition orbital changes for $W = 2$ (MPG)

Video of the dominant dynamical transition orbital changes for $W = 3$ (MPG)

■ AUTHOR INFORMATION

Corresponding Author

Yosuke Kanai − *Department of Chemistry, University of North Carolina at Chapel Hill, Chapel Hill, North Carolina 27599, United States;* orcid.org/0000-0002-2320-4394; Email: ykanai@unc.edu

Authors

Ruiyi Zhou − *Department of Chemistry, University of North Carolina at Chapel Hill, Chapel Hill, North Carolina 27599, United States;* orcid.org/0000-0002-7732-6338

Dillon C. Yost − *Department of Chemistry, University of North Carolina at Chapel Hill, Chapel Hill, North Carolina 27599, United States; Department of Materials Science and Engineering, Massachusetts Institute of Technology, Cambridge, Massachusetts 02139, United States;* orcid.org/0000-0003-0854-1218

Complete contact information is available at: https://pubs.acs.org/10.1021/acs.jpclett.1c01037

Notes

The authors declare no competing financial interest.

■ ACKNOWLEDGMENTS

This work was supported by the National Science Foundation under Award Nos. CHE-1954894 and OAC-17402204. D.C.Y. was supported by an appointment to the Intelligence Community Postdoctoral Research Fellowship Program at Massachusetts Institute of Technology, administered by Oak Ridge Institute for Science and Education through an interagency agreement between the U.S. Department of Energy and the Office of the Director of National Intelligence.

■ REFERENCES

(1) Thouless, D. J. Quantization of Particle Transport. *Phys. Rev. B: Condens. Matter Mater. Phys.* **1983**, *27*, 6083−6087.

(2) Ma, W.; Zhou, L.; Zhang, Q.; Li, M.; Cheng, C.; Geng, J.; Rong, X.; Shi, F.; Gong, J.; Du, J. Experimental Observation of a Generalized Thouless Pump with a Single Spin. *Phys. Rev. Lett.* **2018**, *120*, 120501.

(3) Cerjan, A.; Wang, M.; Huang, S.; Chen, K. P.; Rechtsman, M. C. Thouless Pumping in Disordered Photonic Systems. *Light: Sci. Appl.* **2020**, *9*, 1−7.

(4) Nakajima, S.; Tomita, T.; Taie, S.; Ichinose, T.; Ozawa, H.; Wang, L.; Troyer, M.; Takahashi, Y. Topological Thouless Pumping of Ultracold fermions. *Nat. Phys.* **2016**, *12*, 296.

(5) Lohse, M.; Schweizer, C.; Zilberberg, O.; Aidelsburger, M.; Bloch, I. A Thouless Quantum Pump with Ultracold Bosonic Atoms in an Optical Superlattice. *Nat. Phys.* **2016**, *12*, 350−354.

(6) Hayward, A.; Schweizer, C.; Lohse, M.; Aidelsburger, M.; Heidrich-Meisner, F. Topological Charge Pumping in the Interacting Bosonic Rice-Mele Model. *Phys. Rev. B: Condens. Matter Mater. Phys.* **2018**, *98*, 245148.

(7) Friedman, A. J.; Gopalakrishnan, S.; Vasseur, R. Integrable Many-Body Quantum Floquet-Thouless Pumps. *Phys. Rev. Lett.* **2019**, *123*, 170603.

(8) Taherinejad, M.; Garrity, K. F.; Vanderbilt, D. Wannier Center Sheets in Topological Insulators. *Phys. Rev. B: Condens. Matter Mater. Phys.* **2014**, *89*, 115102.

(9) Li, R.; Fleischhauer, M. Finite-Size Corrections to Quantized Particle Transport in Topological Charge Pumps. *Phys. Rev. B: Condens. Matter Mater. Phys.* **2017**, *96*, 085444.

(10) Guo, A.-M.; Hu, P.-J.; Gao, X.-H.; Fang, T.-F.; Sun, Q.-F. Topological Phase Transitions of Thouless Charge Pumping Realized in Helical Organic Molecules with Long-Range Hopping. *Phys. Rev. B: Condens. Matter Mater. Phys.* **2020**, *102*, 155402.

(11) Zhang, Y.; Gao, Y.; Xiao, D. Topological Charge Pumping in Twisted Bilayer Graphene. *Phys. Rev. B: Condens. Matter Mater. Phys.* **2020**, *101*, 041410.

(12) Rice, M. J.; Mele, E. J. Elementary Excitations of a Linearly Conjugated Diatomic Polymer. *Phys. Rev. Lett.* **1982**, *49*, 1455−1459.

(13) Privitera, L.; Russomanno, A.; Citro, R.; Santoro, G. E. Nonadiabatic Breaking of Topological Pumping. *Phys. Rev. Lett.* **2018**, *120*, 106601.

(14) Kuno, Y. Non-Adiabatic Extension of the Zak Phase and Charge Pumping in the Rice-Mele Model. *Eur. Phys. J. B* **2019**, *92*, 195.

(15) Fedorova, Z.; Qiu, H.; Linden, S.; Kroha, J. In *Topological Transport Quantization by Dissipation in Fast Thouless Pumps*; CLEO: QELS_Fundamental Science, Optical Society of America: 2020; p FM2A. 3.

(16) Oka, T.; Kitamura, S. Floquet Engineering of Quantum Materials. *Annu. Rev. Condens. Matter Phys.* **2019**, *10*, 387−408.

(17) Rudner, M. S.; Lindner, N. H. Band Structure Engineering and Non-Equilibrium Dynamics in Floquet Topological Insulators. *Nature Reviews Physics* **2020**, *2*, 229−244.

(18) Nakagawa, M.; Slager, R.-J.; Higashikawa, S.; Oka, T. Wannier Representation of Floquet Topological States. *Phys. Rev. B: Condens. Matter Mater. Phys.* **2020**, *101*, 075108.

(19) Zel'Dovich, Y. B. The Quasienergy of a Quantum-Mechanical System Subjected to a Periodic Action. *Sov. J Exp. Theor. Phys.* **1967**, *24*, 1006.

(20) Aharonov, Y.; Anandan, J. Phase Change During a Cyclic Quantum Evolution. *Phys. Rev. Lett.* **1987**, *58*, 1593−1596.

(21) Kitagawa, T.; Berg, E.; Rudner, M.; Demler, E. Topological Characterization of Periodically Driven Quantum Systems. *Phys. Rev. B: Condens. Matter Mater. Phys.* **2010**, *82*, 235114.

(22) Xiao, D.; Chang, M.-C.; Niu, Q. Berry Phase Effects on Electronic Properties. *Rev. Mod. Phys.* **2010**, *82*, 1959−2007.

(23) Vanderbilt, D. *Berry Phases in Electronic Structure Theory: Electric Polarization, Orbital Magnetization and Topological Insulators*; Cambridge University Press: Cambridge, 2018.

(24) Yost, D. C.; Yao, Y.; Kanai, Y. Propagation of Maximally Localized Wannier Functions in Real-Time Tddft. *J. Chem. Phys.* **2019**, *150*, 194113.

(25) Marzari, N.; Vanderbilt, D. Maximally Localized Generalized Wannier Functions for Composite Energy Bands. *Phys. Rev. B: Condens. Matter Mater. Phys.* **1997**, *56*, 12847−12865.
(26) Marzari, N.; Mostofi, A. A.; Yates, J. R.; Souza, I.; Vanderbilt, D. Maximally Localized Wannier Functions: Theory and Applications. *Rev. Mod. Phys.* **2012**, *84*, 1419−1475.
(27) Resta, R. Quantum-Mechanical Position Operator in Extended Systems. *Phys. Rev. Lett.* **1998**, *80*, 1800−1803.
(28) Asböth, J. n. K.; Oroszlány, L. S.; Pãlyi, A. S. *A Short Course on Topological Insulators Band Structure and Edge States in One and Two Dimensions*; Springer: Cham; Heidelberg; New York; Dordrecht; London, 2016.
(29) Runge, E.; Gross, E. K. U. Density-Functional Theory for Time-Dependent Systems. *Phys. Rev. Lett.* **1984**, *52*, 997−1000.
(30) Maitra, N. T.; Burke, K. On the Floquet Formulation of Time-Dependent Density Functional Theory. *Chem. Phys. Lett.* **2002**, *359*, 237−240.
(31) Samal, P.; Harbola, M. K. Analysis of Floquet Formulation of Time-Dependent Density-Functional Theory. *Chem. Phys. Lett.* **2006**, *433*, 204−210.
(32) Maitra, N. T.; Burke, K. Comment on "Analysis of Floquet Formulation of Time-Dependent Density-Functional Theory"[Chem. Phys. Lett. 433 (2006) 204]. *Chem. Phys. Lett.* **2007**, *441*, 167−169.
(33) Ullrich, C. A. *Time-Dependent Density-Functional Theory, Concepts and Applications*; Oxford Graduate Texts, 2011.
(34) Marques, M. A.; Gross, E. K. Time-Dependent Density Functional Theory. *Annu. Rev. Phys. Chem.* **2004**, *55*, 427−455.
(35) Krylov, A. I. From Orbitals to Observables and Back. *J. Chem. Phys.* **2020**, *153*, 080901.
(36) Zhou, R.; Kanai, Y. Dynamical Transition Orbitals: A Particle-Hole Description in Real-Time Tddft Dynamics. *J. Chem. Phys.* **2021**, *154*, 054107.
(37) Pendás, A. M.; Contreras-García, J.; Pinilla, F.; Mella, J. D.; Cardenas, C.; Muñoz, F. A Chemical Theory of Topological Insulators. *Chem. Commun.* **2019**, *55*, 12281−12287.
(38) Yabana, K.; Bertsch, G. F. Time-Dependent Local-Density Approximation in Real Time. *Phys. Rev. B: Condens. Matter Mater. Phys.* **1996**, *54*, 4484−4487.
(39) Goings, J. J.; Lestrange, P. J.; Li, X. Real-Time Time-Dependent Electronic Structure Theory. *Wiley Interdiscip. Rev.: Comput. Mol. Sci.* **2018**, *8*, No. e1341.
(40) Li, X.; Govind, N.; Isborn, C.; DePrince III, A. E.; Lopata, K. Real-Time Time-Dependent Electronic Structure Theory. *Chem. Rev.* **2020**, *120*, 9951−9993.
(41) Hübener, H.; Sentef, M. A.; De Giovannini, U.; Kemper, A. F.; Rubio, A. Creating Stable Floquet-Weyl Semimetals by Laser-Driving of 3d Dirac Materials. *Nat. Commun.* **2017**, *8*, 1−8.
(42) Shin, D.; Sato, S. A.; Hübener, H.; De Giovannini, U.; Kim, J.; Park, N.; Rubio, A. Unraveling Materials Berry Curvature and Chern Numbers from Real-Time Evolution of Bloch States. *Proc. Natl. Acad. Sci. U. S. A.* **2019**, *116*, 4135−4140.
(43) Schleife, A.; Draeger, E. W.; Anisimov, V. M.; Correa, A. A.; Kanai, Y. Quantum Dynamics Simulation of Electrons in Materials on High-Performance Computers. *Comput. Sci. Eng.* **2014**, *16*, 54−60.
(44) Francois, G. Architecture of Qbox: A Scalable First-Principles Molecular Dynamics Code. *IBM J. Res. Dev.* **2008**, *52*, 137−144.
(45) Schleife, A.; Draeger, E. W.; Kanai, Y.; Correa, A. A. Plane-Wave Pseudopotential Implementation of Explicit Integrators for Time-Dependent Kohn-Sham Equations in Large-Scale Simulations. *J. Chem. Phys.* **2012**, *137*, 22A546.
(46) Yannoni, C.; Clarke, T. Molecular Geometry of Cis-and Trans-Polyacetylene by Nutation Nmr Spectroscopy. *Phys. Rev. Lett.* **1983**, *51*, 1191.
(47) Hamann, D. R.; Schlüter, M.; Chiang, C. Norm-Conserving Pseudopotentials. *Phys. Rev. Lett.* **1979**, *43*, 1494−1497.
(48) Vanderbilt, D. Optimally Smooth Norm-Conserving Pseudopotentials. *Phys. Rev. B: Condens. Matter Mater. Phys.* **1985**, *32*, 8412−8415.
(49) Perdew, J. P.; Burke, K.; Ernzerhof, M. Generalized Gradient Approximation Made Simple. *Phys. Rev. Lett.* **1996**, *77*, 3865−3868.
(50) Castro, A.; Marques, M. A.; Rubio, A. Propagators for the Time-Dependent Kohn-Sham Equations. *J. Chem. Phys.* **2004**, *121*, 3425−3433.

https://doi.org/10.1021/acs.jpclett.1c01037
J. Phys. Chem. Lett. 2021, 12, 4496−4503